A stochastic Galerkin method for the direct and inverse random source problems of the Helmholtz equation

Ning Guan * Dingyu Chen † Peijun Li ‡ Xinghui Zhong §

Abstract

This paper investigates a novel approach for solving both the direct and inverse random source problems of the one-dimensional Helmholtz equation with additive white noise, based on the generalized polynomial chaos (gPC) approximation. The direct problem is to determine the wave field that is emitted from a random source, while the inverse problem is to use the boundary measurements of the wave field at various frequencies to reconstruct the mean and variance of the source. The stochastic Helmholtz equation is reformulated in such a way that the random source is represented by a collection of mutually independent random variables. The stochastic Galerkin method is employed to transform the model equation into a two-point boundary value problem for the gPC expansion coefficients. The explicit connection between the sine or cosine transform of the mean and variance of the random source and the analytical solutions for the gPC coefficients is established. The advantage of these analytical solutions is that the gPC coefficients are zero for basis polynomials of degree higher than one, which implies that the total number of the gPC basis functions increases proportionally to the dimension, and indicates that the stochastic Galerkin method has the potential to be used in practical applications involving random variables of higher dimensions. By taking the inverse sine or cosine transform of the data, the inverse problem can be solved, and the statistical information of the random source such as the mean and variance can be obtained straightforwardly as the gPC basis functions are orthogonal. Numerical experiments are conducted to demonstrate the efficiency of the proposed method.

Keywords: Generalized polynomial chaos, the Helmholtz equation, inverse random source problem, stochastic Galerkin method, uncertainty quantification

AMS subject classification: 34A55, 65C30, 65L09, 78A46

1 Introduction

The inverse source problem for wave equations seeks to identify unknown sources that generate a given wave pattern. This has numerous applications in scientific fields such as medical imaging,

*School of Mathematical Sciences, Zhejiang University, Hangzhou, 310027, China. adaguann99@zju.edu.cn
†School of Mathematical Sciences, Zhejiang University, Hangzhou, 310027, China. musisoul@zju.edu.cn
‡Department of Mathematics, Purdue University, West Lafayette, Indiana 47907. lipeijun@math.purdue.edu
§School of Mathematical Sciences, Zhejiang University, Hangzhou, 310027, China. zhongxh@zju.edu.cn

where the aim is to use measurements of the electric or magnetic field on the body's surface to figure out the source currents inside [2]. Over the past few decades, there have been numerous mathematical and numerical studies of the inverse source problem for acoustic and electromagnetic wave equations [1, 3, 12]. It is known that nonradiating sources can exist, for which the resulting wave field is zero outside a finite region [9]. Consequently, the fixed frequency does not yield a unique solution to the inverse source problem. To address this issue, multi-frequency data can be used to gain uniqueness and increase stability [8, 13]. A comprehensive review of solving inverse scattering problems for wave equations with multi-frequencies can be found in [7].

In practice, mathematical models often contain uncertainties arising from random surrounding environments [14]. To represent these uncertainties, random parameters are introduced. While the deterministic counterparts have been widely studied, the stochastic inverse source problems have been largely neglected. Early work [11] showed that the auto-correlation of the random source can be uniquely determined by the radiating field outside the source region. Subsequent research [5, 6, 20, 21] developed an effective computational model for the inverse random source problem of the one-dimensional Helmholtz equation driven by additive white noise, and extended it to higher dimensional problems in homogeneous and inhomogeneous media. More recently, the model of the microlocally isotropic Gaussian field was developed in [19, 22] to handle more general stochastic processes with correlated increments, and some uniqueness results were established to determine the micro-correlation strength of the principal symbol of the covariance operator for the random parameters. For further information, we refer to the monograph [17] on statistical and computational methods for inverse problems involving uncertainties and randomness.

In this paper, we present a novel approach to solve the direct and inverse random source problems of the one-dimensional Helmholtz equation driven by an additive white noise, based on the generalized polynomial chaos (gPC) approximation. Wiener first introduced the concept of polynomial chaos (PC) in his work [27], where he studied the decomposition of Gaussian random processes with Hermite polynomials as an orthogonal basis. Ghanem and his collaborators then developed the original PC method, which uses Hermite polynomials to model uncertainties as Gaussian processes [15]. Xiu and Karniadakis further proposed the gPC method [29], which uses different orthogonal polynomials as a basis depending on the probability distribution of the random inputs and is capable of representing more general random processes. This method is mathematically robust and can be implemented numerically with either stochastic Galerkin methods or stochastic collocation methods [28]. Related work can be found in [4, 10, 16, 25, 26] for numerical solutions of the stochastic Helmholtz equation.

This paper investigates numerical solutions to the direct and inverse random source problems for the one-dimensional Helmholtz equation in a homogeneous medium. The random source is generated by Gaussian random processes and is assumed to be supported in a finite interval. The boundary condition of outgoing radiation is applied to the two endpoints of a finite interval. The direct problem is to identify the radiating wave field when a random source is present, while the inverse problem involves calculating the mean and variance of a random source from the boundary measurements of the wave field across a range of frequencies. Inspired by [6], which demonstrated that the direct problem can be transformed into an equivalent first order stochastic two-point boundary value problem and that it has a unique pathwise solution for each realization of the random field, we explore

the stochastic Galerkin method for this model problem. The random source is characterized by a set of mutually independent random variables, which allows us to reformulate the stochastic Helmholtz equation. The stochastic Galerkin method is then employed, with the gPC basis functions being orthogonal polynomials based on the distribution of the random variables. This is followed by a Galerkin projection of the stochastic model equation. The model problem is now expressed as a set of deterministic equations regarding the coefficients of the gPC expansion. Analytical solutions to the gPC coefficients are deduced, with those of basis polynomials of degree higher than one being zero. This ensures that the total number of gPC basis functions increases in line with the dimension, and further indicates that the stochastic Galerkin method has a lot of potential for practical applications involving higher-dimensional random variables. Additionally, the gPC coefficients for the random wave field are explicitly linked to the sine or cosine transform of the mean and variance of the random source. The orthogonality of the gPC basis functions makes it easy to obtain the mean and variance of the random source from the boundary measurements of the wave field across a range of frequencies. The numerical results of this paper show that the method is both precise and reliable for both direct and inverse random source problems. Furthermore, since it is a gPC approximation, the results are also applicable to inverse random source problems driven by more complex stochastic processes, and can be used as a guide when the gPC approach is used to solve other stochastic inverse problems.

The paper is structured as follows. Section 2 presents the stochastic model problem and reviews the solutions for the corresponding deterministic problem. The stochastic Galerkin method of the gPC approximation is then proposed for the direct and inverse random source problems. Section 3 presents numerical experiments of the direct and inverse source problems. Finally, Section 4 offers general remarks and directions for future work.

2 Direct and inverse source problems

This section analyzes the direct and inverse source problems for the one-dimensional stochastic Helmholtz equation. To numerically solve these problems, we introduce the stochastic Galerkin method.

2.1 Problem formulation

The one-dimensional stochastic Helmholtz equation in a homogeneous medium can be expressed as

$$u''(x,\omega) + \omega^2 u(x,\omega) = f(x), \quad x \in (0,1), \tag{2.1}$$

where $\omega > 0$ is the angular frequency, u is the radiating wave field, and the source f is a random field that represents the electric current density. For the sake of simplicity, the magnetic permeability and the electric permittivity of the medium are assumed to be equal to one. Moreover, we assume that the random source f is given by

$$f(x) = g(x) + h(x)\dot{W}(x), \tag{2.2}$$

where g and h are deterministic real-valued functions compactly supported in $[0, 1]$, and $\dot{W}(x)$ is the white noise with $W(x)$ being the Brownian motion [18]. It is evident from (2.2) that the mean and variance of f are given by

$$\mathbb{E}[f(x)] = g(x), \quad \mathbb{V}[f(x)] = h^2(x).$$

The outgoing radiation condition requires that u satisfies

$$u'(0, \omega) + \mathrm{i}\omega u(0, \omega) = 0, \quad u'(1, \omega) - \mathrm{i}\omega u(1, \omega) = 0, \tag{2.3}$$

which indicates the presence of a left-going wave at $x = 0$ and a right-going wave at $x = 1$, respectively. As demonstrated in [6], the two-point stochastic boundary value problem (2.1) and (2.3) admits a mild solution of the form

$$u(x, \omega) = \frac{1}{2\mathrm{i}\omega} \int_0^1 e^{\mathrm{i}\omega|x-y|} g(y)dy + \frac{1}{2\mathrm{i}\omega} \int_0^1 e^{\mathrm{i}\omega|x-y|} h(y)dW(y). \tag{2.4}$$

The inverse problem involves reconstructing the mean g and variance h^2 of the random source f from the measured wave field on $x = 0$ or $x = 1$ at a finite number of angular frequencies ω. This is in contrast to the direct problem, which is to determine the radiating wave field u given the mean and variance of the source. In this paper, we consider numerical solutions to both the direct and inverse source problems by employing the stochastic Galerkin method.

2.2 Deterministic source problems

We provide a brief overview of the solutions to the direct and inverse source problems for the deterministic Helmholtz equation.

When $h = 0$, the stochastic Helmholtz equation (2.1) reduces to

$$u''(x, \omega) + \omega^2 u(x, \omega) = g(x), \tag{2.5}$$

where the radiating wave field u is also required to satisfy the outgoing wave boundary conditions

$$u'(0, \omega) + \mathrm{i}\omega u(0, \omega) = 0, \quad u'(1, \omega) - \mathrm{i}\omega u(1, \omega) = 0. \tag{2.6}$$

It is straightforward to verify that the one-dimensional Helmholtz problem (2.5)–(2.6) admits a unique solution, which is expressed as

$$u(x, \omega) = \frac{1}{2\mathrm{i}\omega} \int_0^1 e^{\mathrm{i}\omega|x-y|} g(y)dy. \tag{2.7}$$

Following [6], we evaluate (2.7) on both sides at $x = 0$ and obtain

$$2\mathrm{i}\omega u(0, \omega) = \int_0^1 e^{\mathrm{i}\omega y} g(y)dy. \tag{2.8}$$

Let $u(0, \omega) = \Re u(0, \omega) + \mathrm{i}\Im u(0, \omega)$. A simple calculation from (2.8) gives

$$2\omega \Re u(0, \omega) = \int_0^1 \sin(\omega y) g(y)dy, \quad 2\omega \Im u(0, \omega) = -\int_0^1 \cos(\omega y) g(y)dy. \tag{2.9}$$

If the wave field u is measured at $x = 0$ and angular frequencies $\omega_k = k\pi, k \in \mathbb{Z}^+$, then the source function g can be recovered from either the inverse sine or cosine transform via

$$g(x) = \sum_{k=1}^{\infty} 4\omega_k \Re u(0, \omega_k) \sin(\omega_k x), \quad g(x) = -\sum_{k=1}^{\infty} 4\omega_k \Im u(0, \omega_k) \cos(\omega_k x). \tag{2.10}$$

It is important to note that (2.9) is only applicable for $\omega > 0$, which is a positive frequency. The zero Fourier mode is not included, which results in the reconstruction not being unique; the reconstructed function, when shifted vertically, will still generate the same Fourier modes that are associated with the positive frequencies. In practice, the Fourier mode that is equal to zero is usually disregarded. In order to make the value of the reconstructed function vanish at the end points $x = 0$ or $x = 1$ for the inverse cosine transform in (2.10), an artificial shift in the vertical direction must be applied since g is assumed to be compact in the interval $[0, 1]$. For the inverse sine transform in (2.10), the zero Fourier mode, i.e., $\omega = 0$, has no contribution to the reconstructed function. Therefore, for simplicity, the inverse sine transform is used for reconstruction in the rest of the paper. All the discussions hold true for the inverse cosine transform with a shift in the vertical direction. It is worth mentioning that the left boundary point $x = 0$ is used for the presentation in the paper. All the results remain valid if the wave field is measured at the right boundary point $x = 1$.

2.3 Random source problems

In this section, we analyze the direct and inverse random source problems by characterizing the stochastic process with a set of mutually independent random variables.

Let us begin with a representation of the white noise $\dot{W}(x)$, which is an infinite-dimensional stochastic process. Since $\dot{W}(x)$ is a Gaussian random process, it has an orthogonal expansion (cf. [24])

$$W(x) = \sum_{k=1}^{\infty} Z_k \int_0^x m_k(y)dy, \quad \dot{W}(x) = \sum_{k=1}^{\infty} Z_k m_k(x), \quad x \in (0, 1), \tag{2.11}$$

where $\{m_k(x)\}_{k=1}^{\infty}$ is a complete orthonormal basis in $L^2([0, 1])$, and $\{Z_k\}_{k=1}^{\infty}$ are mutually independent standard Gaussian random variables. In practice, $\dot{W}(x)$ can be approximated by a truncated series

$$\dot{W}(x) \approx W_n = \sum_{k=1}^{n} m_k(x) Z_k, \tag{2.12}$$

where n is the number of random variables. Clearly, it leads to a different representation by using a different choice of orthonormal basis. Instead of engaging in depth discussion of this issue, we refer to [30] for the detailed study on error estimates and convergence analysis for the white noise.

When discretizing a random process into a finite-dimensional approximation, the finer the discretization is, the more accurate the approximation is. However, a finer discretization leads to a larger dimension in random space and can significantly increase the computational complexity. To reduce the dimension while maintaining a satisfactory approximation accuracy, dimension reduction techniques such as the Karhunen–Loève (KL) expansion [23] can be employed. The KL expansion

of a random process $W(x)$ can be represented by a set of mutually uncorrelated random variables. Specifically, the KL expansion of $X(x)$ is given by

$$W(x) = \sum_{k=1}^{\infty} \sqrt{\lambda_k}\psi_k(x)Z_k,$$

where $\psi_k(x)$ and λ_k are the orthogonal eigenfunctions and the corresponding eigenvalues of the following eigenvalue problem:

$$\int_0^1 C(x,y)\psi_k(x)dx = \lambda_k\psi_k(x), \quad C(x,y) = \mathrm{cov}(W(x), W(y)), \tag{2.13}$$

and the sequence of random variables $\{Z_k\}_{k=1}^{\infty}$ have no correlation between them and each has a mean of zero and a variance of one, i.e.,

$$\mathbb{E}[Z_k] = 0, \quad \mathbb{E}[Z_k Z_j] = \delta_{kj},$$

where δ_{kj} is the Kronecker delta function. The random variables Z_k are given by

$$Z_k = \frac{1}{\sqrt{\lambda_k}} \int_0^1 (W(x) - \mathbb{E}[W(x)])\psi_k(x)dx.$$

It can be verified that the eigenfunctions and the corresponding eigenvalues of (2.13) for the Brownian motion $W(x)$ with $\mathrm{cov}(W(x), W(y)) = \min(x, y)$ are given by

$$\psi_k(x) = \sqrt{2}\sin\Big((k-\frac{1}{2})\pi x\Big), \qquad \lambda_k = \frac{1}{(k-\frac{1}{2})^2\pi^2}.$$

Therefore, the KL expansion of the Brownian motion $W(x)$ is expressed as

$$W(x) = \sqrt{2}\sum_{k=1}^{\infty} \frac{\sin((k-\frac{1}{2})\pi x)}{(k-\frac{1}{2})\pi} Z_k,$$

where $\{Z_k\}$ are now mutually independent standard Gaussian random variables since uncorrelation and independence are equivalent to Gaussian distributions. White noise can be defined mathematically as

$$\dot{W}(x) = \sum_{k=1}^{\infty} \sqrt{2}\cos\Big((k-\frac{1}{2})\pi x\Big)Z_k,$$

which is equivalent to the representation of (2.11) when $m_k(x) = \sqrt{2}\cos\Big((k-\frac{1}{2})\pi x\Big)$, and is used in our numerical experiments.

Let $\mathbf{Z} = (Z_1, \ldots, Z_n)$ be an n-dimensional standard Gaussian random variable, i.e., $Z_k \sim \mathcal{N}(0,1)$ for $k = 1, \ldots, n$. Using the parametrization W_n of $\dot{W}(x)$ in (2.12), we can reformulate the stochastic Helmholtz equation (2.1) as

$$u''(x,\omega,\mathbf{Z}) + \omega^2 u(x,\omega,\mathbf{Z}) = g(x) + h(x)W_n, \quad x \in (0,1), \tag{2.14}$$

where u satisfies the same outgoing radiation boundary condition

$$u'(0,\omega,\mathbf{Z}) + \mathrm{i}\omega u(0,\omega,\mathbf{Z}) = 0, \quad u'(1,\omega,\mathbf{Z}) - \mathrm{i}\omega u(1,\omega,\mathbf{Z}) = 0. \tag{2.15}$$

2.4 The stochastic Galerkin method

In this section, we present the stochastic Galerkin method for discretizing the stochastic model (2.14)–(2.15) in the random space, and investigate the direct and inverse source problems in the context of this model.

Following the standard gPC method [29], we employ the Hermite orthogonal polynomials as the gPC basis functions, which is also the classical Wiener polynomial chaos basis [15]. Let $H_j(Z_k)$ be the univariate Hermite orthonormal polynomial in Z_k of degree j, which satisfies

$$\int_{-\infty}^{\infty} H_j(Z_k)H_i(Z_k)\rho(Z_k)dZ_k = \delta_{ji},$$

where $\rho(Z_k) = \frac{1}{\sqrt{2\pi}}e^{-Z_k^2/2}$ is the probability distribution function of the standard Gaussian random variable. The polynomials are normalized here for simplicity. For example, the first few polynomials are listed as follows:

$$H_0(Z_k) = 1, \quad H_1(Z_k) = Z_k, \quad H_2(Z_k) = \frac{1}{2}(Z_k^2 - 1). \tag{2.16}$$

The n-variate N-th degree Hermite polynomials are the tensor products of the univariate Hermite orthonormal polynomials of total degree less than or equal to N, i.e.,

$$\mathbf{H_j}(\mathbf{Z}) = H_{j_1}(Z_1)H_{j_2}(Z_2)\cdots H_{j_n}(Z_n), \quad 0 \le |\mathbf{j}| \le N,$$

where $\mathbf{j} = (j_1, \ldots, j_n)$ is a multi-index and $|\mathbf{j}| = j_1 + j_2 + \cdots + j_n$. The truncated white noise W_n in (2.12) can be expressed as

$$W_n(x, \mathbf{Z}) = \sum_{k=1}^{n} m_k(x)Z_k = \sum_{|\mathbf{j}|=1} \hat{m}_{\mathbf{j}}(x)\mathbf{H_j}(\mathbf{Z}), \tag{2.17}$$

where $\hat{m}_{\mathbf{j}}(x) = \mathbb{E}[W_n(x, \mathbf{Z})\mathbf{H_j}(\mathbf{Z})]$.

For any fixed (x, ω), the stochastic Galerkin method seeks an approximation to the solution $u(x, \omega, \mathbf{Z})$ via a finite-term gPC expression

$$u_N(x, \omega, \mathbf{Z}) = \sum_{|\mathbf{j}|=0}^{N} \hat{u}_{\mathbf{j}}(x, \omega)\mathbf{H_j}(\mathbf{Z}). \tag{2.18}$$

Substituting (2.17)–(2.18) into (2.14) and conducting the Galerkin projection of the resulting equation onto the subspace spanned by the gPC basis polynomials, i.e., span$\{\mathbf{H}_0(\mathbf{Z}), \ldots, \mathbf{H}_N(\mathbf{Z})\}$, we have

$$\begin{aligned}\mathbb{E}\left[\left(\sum_{|\mathbf{j}|=0}^{N} \hat{u}''_{\mathbf{j}}(x, \omega)\mathbf{H_j}(\mathbf{Z})\right)\mathbf{H_k}(\mathbf{Z})\right] + \omega^2\mathbb{E}\left[\left(\sum_{|\mathbf{j}|=0}^{N} \hat{u}_{\mathbf{j}}(x, \omega)\mathbf{H_j}(\mathbf{Z})\right)\mathbf{H_k}(\mathbf{Z})\right] \\ = \mathbb{E}\left[\left(g(x) + h(x)\sum_{|\mathbf{j}|=1} \hat{m}_{\mathbf{j}}(x)\mathbf{H_j}(\mathbf{Z})\right)\mathbf{H_k}(\mathbf{Z})\right],\end{aligned}$$

where the multi-index $\mathbf{k} = (k_1, \ldots, k_n)$ with $|\mathbf{k}| = 0, 1, \ldots, N$. It follows from the orthonormal property of the gPC basis that

$$\hat{u}''_{\mathbf{k}}(x,\omega) + \omega^2 \hat{u}_{\mathbf{k}}(x,\omega) = \begin{cases} g(x), & |\mathbf{k}| = 0, \\ h(x)\hat{m}_{\mathbf{k}}(x), & |\mathbf{k}| = 1, \\ 0, & 2 \le |\mathbf{k}| \le N, \end{cases} \tag{2.19}$$

which is a deterministic system for the expansion coefficients. The boundary condition can be similarly obtained by the gPC projection of (2.15):

$$\hat{u}'_{\mathbf{k}}(0,\omega) + \mathrm{i}\omega \hat{u}_{\mathbf{k}}(0,\omega) = 0, \quad \hat{u}'_{\mathbf{k}}(1,\omega) - \mathrm{i}\omega \hat{u}_{\mathbf{k}}(1,\omega) = 0, \quad |\mathbf{k}| = 0, 1, \ldots, N. \tag{2.20}$$

Proposition 1. The gPC expansion coefficients in (2.18) can be explicitly expressed as

$$\hat{u}_{\mathbf{k}}(x,\omega) = \begin{cases} \dfrac{1}{2\mathrm{i}\omega} \displaystyle\int_0^1 e^{\mathrm{i}\omega|x-y|} g(y)dy, & |\mathbf{k}| = 0, \\ \dfrac{1}{2\mathrm{i}\omega} \displaystyle\int_0^1 e^{\mathrm{i}\omega|x-y|} h(y)\hat{m}_{\mathbf{k}}(y)dy, & |\mathbf{k}| = 1, \\ 0, & 2 \le |\mathbf{k}| \le N. \end{cases} \tag{2.21}$$

Proof. For $|\mathbf{k}| = 0$, it follows from (2.19) that

$$\hat{u}''_{\mathbf{k}}(x,\omega) + \omega^2 \hat{u}_{\mathbf{k}}(x,\omega) = g(x),$$

which, combining with the boundary conditions (2.20), has the solution

$$\hat{u}_{\mathbf{k}}(x,\omega) = \frac{1}{2\mathrm{i}\omega} \int_0^1 e^{\mathrm{i}\omega|x-y|} g(y)dy.$$

Similarly, for $|\mathbf{k}| = 1$, the deterministic system for the gPC coefficients is

$$\hat{u}''_{\mathbf{k}}(x,\omega) + \omega^2 \hat{u}_{\mathbf{k}}(x,\omega) = h(x)\hat{m}_{\mathbf{k}}(x),$$

which, together with the boundary conditions (2.20), yields

$$\hat{u}_{\mathbf{k}}(x,\omega) = \frac{1}{2\mathrm{i}\omega} \int_0^1 e^{\mathrm{i}\omega|x-y|} h(y)\hat{m}_{\mathbf{k}}(y)dy.$$

For $|\mathbf{k}| \ge 2$, it is easy to verify that the homogeneous system

$$\hat{u}''_{\mathbf{k}}(x,\omega) + \omega^2 \hat{u}_{\mathbf{k}}(x,\omega) = 0$$

and the boundary conditions (2.20) give $\hat{u}_{\mathbf{k}} = 0$, which completes the proof. □

By Proposition 1, the gPC coefficients are zero for the polynomial basis of degree higher than one. Based on the stochastic Galerkin method, the solution of (2.14)–(2.15) is

$$u_N(x,\omega,\mathbf{Z}) = \sum_{|\mathbf{k}|=0,1} \hat{u}_{\mathbf{k}}(x,\omega)\mathbf{H}_{\mathbf{k}}(\mathbf{Z}), \tag{2.22}$$

which is an n-variate first degree polynomial approximation. It is known from the tensor product construction that the total number of the gPC basis functions for the N-degree of the gPC expansion with n random variables grows exponentially fast at the rate of N^n as the number of random parameters n grows, which is called the curse of dimensionality. However, it follows from Proposition 1 that for the N-degree of the gPC expansion in (2.18) with n random variables, the number of basis functions is $n+1$ and is independent of N. Therefore, the number of basis functions grows at the same rate as the dimension, which provides great potential to apply the stochastic Galerkin method in practical applications involving higher-dimensional random variables.

For simplicity, we rewrite (2.22) with a single-index in the graded lexicographic order

$$u_n(x,\omega,\mathbf{Z}) = \hat{u}_0(x,\omega) + \sum_{k=1}^{n} \hat{u}_k(x,\omega)H_1(Z_k), \tag{2.23}$$

which is more convenient to be implemented in practice. Hereafter, We use the notation u_n to denote u_N without ambiguity. Similarly, the expansion coefficients in (2.21) can also be rewritten in the single-index form

$$\hat{u}_k(x,\omega) = \begin{cases} \dfrac{1}{2\mathrm{i}\omega}\displaystyle\int_0^1 e^{\mathrm{i}\omega|x-y|}g(y)dy, & k=0, \\ \dfrac{1}{2\mathrm{i}\omega}\displaystyle\int_0^1 e^{\mathrm{i}\omega|x-y|}h(y)m_k(y)dy, & 1\le k\le n. \end{cases} \tag{2.24}$$

For the direct random source problem, the numerical solution can be directly obtained from (2.23) and (2.24). Moreover, the solution (2.23) is an analytical representation in terms of $\mathbf{Z}$, and thus all the statistical information can be retrieved either analytically or computationally with a minimal effort. By the orthogonality of the gPC basis functions, the mean and variance of the gPC solution u_n in (2.23) can be computed by

$$\mathbb{E}[u_n] = \hat{u}_0, \quad \mathbb{V}[u_n] = \sum_{k=1}^{n} \hat{u}_k^2, \tag{2.25}$$

respectively.

For the inverse random source problem, the boundary measurements $u(0,\omega,\mathbf{Z})$ are assumed to be available at a finite number of angular frequencies. The gPC basis functions are associated with the probability distribution of $\mathbf{Z}$. If we assume $F_{\mathbf{Z}}$ is the probability distribution of the random vector $\mathbf{Z}$ in a properly defined complete probability space $\Omega_{\mathbf{Z}}$, the gPC basis functions are chosen to be orthogonal polynomials satisfying

$$\int_{\Omega_{\mathbf{Z}}} \Phi_{\mathbf{j}}(\mathbf{Z})\Phi_{\mathbf{k}}(\mathbf{Z})dF_{\mathbf{Z}}(\mathbf{Z}) = \delta_{\mathbf{jk}},$$

where $\delta_{\mathbf{jk}} = \delta_{j_1k_1} \cdots \delta_{j_nk_n}$. The polynomials used as a basis are normalized for convenience and are determined by the distribution of the random variable $\mathbf{Z}$. For instance, the Legendre polynomials are linked to uniform distributions, and the Hermite polynomials are related to Gaussian distributions. We refer to [28, 29] for a more detailed discussion on numerical methods, particularly the gPC method, to solve stochastic differential equations.

With $\{\Phi_{\mathbf{j}}(\mathbf{Z})\}$ serving as the gPC basis, the procedure to obtain the two-point boundary value problem for gPC coefficients is similar to that with $\mathbf{H}_{\mathbf{j}}(\mathbf{Z})$, and the gPC coefficients can also be explicitly expressed as in Proposition 1. To simplify the presentation, we assume that the random vector $\mathbf{Z}$ in the boundary measurements $u(0, \omega, \mathbf{Z})$ is an n-dimensional Gaussian random vector and the gPC basis functions are Hermite polynomials. Evaluating (2.23) and (2.24) on both sides at $x = 0$ yields

$$u_n(0, \omega, \mathbf{Z}) = \hat{u}_0(0, \omega) + \sum_{k=1}^{n} \hat{u}_k(0, \omega) H_1(Z_k),$$

where the expansion coefficients are given by

$$\hat{u}_k(0, \omega) = \begin{cases} \dfrac{1}{2\mathrm{i}\omega} \displaystyle\int_0^1 e^{\mathrm{i}\omega y} g(y) dy, & k = 0, \\ \dfrac{1}{2\mathrm{i}\omega} \displaystyle\int_0^1 e^{\mathrm{i}\omega y} h(y) m_k(y) dy, & 1 \le k \le n. \end{cases} \tag{2.26}$$

Let $\hat{u}_k(0, \omega) = \Re\hat{u}_k(0, \omega) + \mathrm{i}\Im\hat{u}_k(0, \omega), k = 0, 1, \ldots, n$. Splitting (2.26) into the real and imaginary parts, we get

$$2\omega\Re\hat{u}_0(0, \omega) = \int_0^1 \sin(\omega y) g(y) dy, \quad 2\omega\Im\hat{u}_0(0, \omega) = -\int_0^1 \cos(\omega y) g(y) dy \tag{2.27}$$

and

$$2\omega\Re\hat{u}_k(0, \omega) = \int_0^1 \sin(\omega y) h(y) m_k(y) dy, \quad 2\omega\Im\hat{u}_k(0, \omega) = -\int_0^1 \cos(\omega y) h(y) m_k(y) dy. \tag{2.28}$$

Given the measured wave field $u(0, \omega, \mathbf{Z})$ at a range of frequencies, i.e., $u(0, \omega_j, \mathbf{Z})$, $j = 1, \ldots, n_\omega$, the coefficients of its gPC expansion can be computed by

$$\hat{u}_0(0, \omega_j) = \mathbb{E}[u(0, \omega_j, \mathbf{Z}) H_0(Z_k)], \quad \hat{u}_k(0, \omega_j) = \mathbb{E}[u(0, \omega_j, \mathbf{Z}) H_1(Z_k)], \tag{2.29}$$

for $k = 1, \ldots, n$, where $H_0(Z_k)$ and $H_1(Z_k)$ are orthonormal Hermite polynomials defined in (2.16).

The mean $g(x)$ can be recovered from the inverse sine transform via

$$g(x) = \sum_{j=1}^{n_\omega} 4\omega_j \Re\hat{u}_0(0, \omega_j) \sin(\omega_j x).$$

Similarly, the functions $h(x)m_k(x)$, for $k = 1, \ldots, n$, can be recovered using the inverse sine transform via

$$h(x)m_k(x) = \sum_{j=1}^{n_\omega} 4\omega_j \Re\hat{u}_k(0, \omega_j) \sin(\omega_j x). \tag{2.30}$$

Recalling that h is deterministic and compactly supported in (0,1), and that $\{m_k(x)\}_{k=1}^{\infty}$ forms a complete orthonormal basis in $L^2([0,1])$, we can obtain the expansion $h(x) = \sum_{k=1}^{\infty} \hat{h}_k m_k(x)$, where $\hat{h}_k = \int_0^1 h(x)m_k(x)\,dx$. It follows from (2.30) that

$$\hat{h}_k = \int_0^1 \left(\sum_{j=1}^{n_\omega} 4\omega_j \Re\hat{u}_k(0, \omega_j) \sin(\omega_j x) \right) dx = \sum_{j=1}^{n_\omega} 4\Re\hat{u}_k(0, \omega_j) \Big(1 - \cos(\omega_j)\Big)$$

holds for $k = 0, 1, \ldots, n$, where $\Re\hat{u}_k(0, \omega_j)$ are the real part of $\hat{u}_k(0, \omega_j)$ given in (2.29). Then $h(x)$ can be approximated by

$$h(x) \approx \sum_{k=0}^{n} \hat{h}_k m_k(x) = \sum_{k=0}^{n} \sum_{j=1}^{n_\omega} 4\Re\hat{u}_k(0, \omega_j) \Big(1 - \cos(\omega_j)\Big) m_k(x),$$

and the variance $h^2(x)$ can be recovered accordingly.

3 Numerical experiments

In this section, we adopt the examples from [6] to demonstrate the performance of the stochastic Galerkin method for both the direct and inverse random source problems. It is worth emphasizing that, unlike the sampling method, the statistical information such as the mean and variance of the results obtained from the gPC approach can be computed in a straightforward manner using (2.25).

3.1 Direct random source problem

In the following numerical experiments, we examine errors in the mean and variance of the numerical solution for the direct problem. It follows from (2.21) and (2.25) that the mean of the solution is exactly the first coefficient of the gPC expansion and is independent of the number of random variables n, which is also the dimension of the random space in our stochastic model (2.14). Therefore, we only document the error in the variance of the gPC solution with respect to n. The variance of the exact solution (2.4) can be obtained by the Itô isometry

$$\mathbb{V}[\Re u(x, \omega)] = \frac{1}{8\omega^2} \int_0^1 (1 - \cos(2\omega|x - y|))\, h^2(y) dy, \tag{3.1}$$

$$\mathbb{V}[\Im u(x, \omega)] = \frac{1}{8\omega^2} \int_0^1 (1 + \cos(2\omega|x - y|))\, h^2(y) dy. \tag{3.2}$$

For all three examples, we test the numerical solutions obtained with the truncation of the white noise defined in (2.12) using both $m_k(x) = \sqrt{2}\cos((k-1/2)\pi x)$ and $m_k(x) = \sqrt{2}\sin((k-1/2)\pi x)$. We obtain equally good results for both cases, so we only show the results obtained by $m_k(x) = \sqrt{2}\cos((k-1/2)\pi x)$. We fix $\omega = 3\pi$ unless otherwise specified.

Example 1. In this example, the mean g and standard deviation h of the random source f are taken as

$$g(x) = \hat{g}(2\pi x), \qquad h(x) = \hat{h}(2\pi x), \tag{3.3}$$

where

$$\hat{g}(x) = 0.3\left[(1-\cos(2x)) - \frac{16}{21}(1-\cos(3x)) + \frac{5}{28}(1-\cos(4x))\right],$$
$$\hat{h}(x) = 0.6 - 0.3\cos(x) - 0.3\cos(2x).$$

In Figure 3.1, the numerical solution with $n = 20$ is plotted against the exact solution for the variance of the real and imaginary parts of the wave field. It is evident that the results obtained by the stochastic Galerkin method agree well with the results of the exact solution. In Figure 3.2, which is presented as a semi-log scale, the L_1 and L_∞ errors in the variance for the real and imaginary parts of the wave field are plotted with respect to the number of random variables n. Here, the case with $\omega = 3.5\pi$ is further investigated for a comparison of the solutions at different frequencies. It can be seen that exponential convergence is achieved with respect to the dimension of the random space for different frequencies ω.

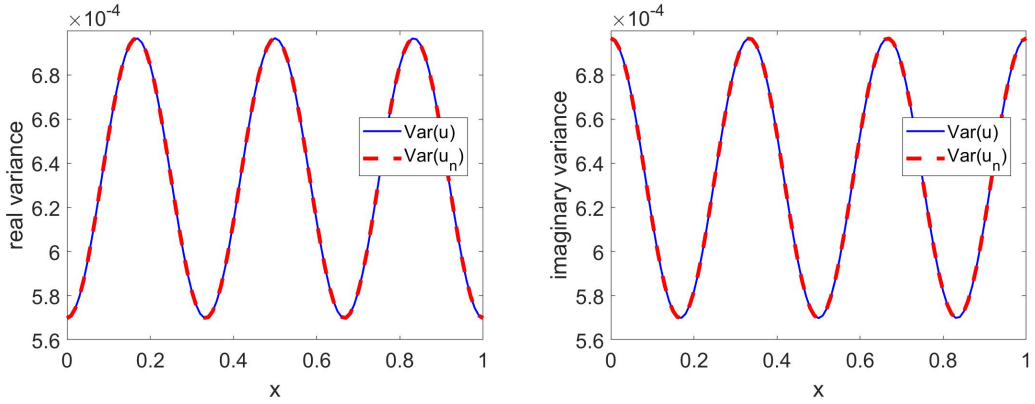

Figure 3.1: Example 1. The numerical solution (red dashed line) and the exact solution (blue solid line) for the variance (bottom) of the real (left) and imaginary (right) parts of the wave field.

Example 2. In this example, the random source f is given by

$$g(x) = \hat{g}(2\pi x), \qquad h(x) = \hat{h}(2\pi x), \tag{3.4}$$

where

$$\hat{g}(x) = 0.4\left[(1-\cos(3x)) - \frac{1215}{2783}(1-\cos(11x)) + \frac{7}{23}(1-\cos(12x))\right],$$
$$\hat{h}(x) = 0.5e^{1} - 0.3e^{\cos(2x)} - 0.2e^{\cos(3x)},$$

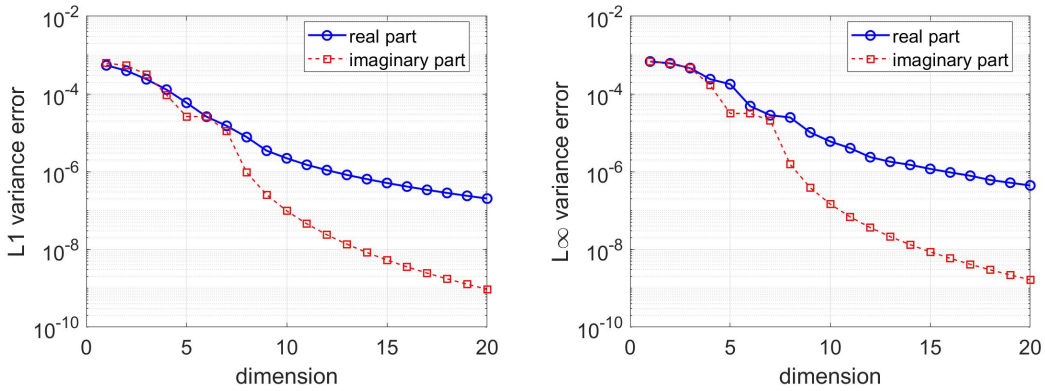

(a) $\omega = 3\pi$ (b) $\omega = 3\pi$

(c) $\omega = 3.5\pi$ (d) $\omega = 3.5\pi$

Figure 3.2: Example 1. L_1 (left) and L_∞ (right) errors in the variance of real and imaginary parts of the wave field with respect to the dimension of the random space at $\omega = 3\pi$ (top) and $\omega = 3.5\pi$ (bottom).

where g and h containing higher frequency models compared with Example 1.

In Figure 3.3, we plot the L_1 and L_∞ errors in the variance of the real and imaginary parts of the wave field with respect to the dimension of the random space. As expected, we observe an exponential convergence with respect to the dimension of the random space.

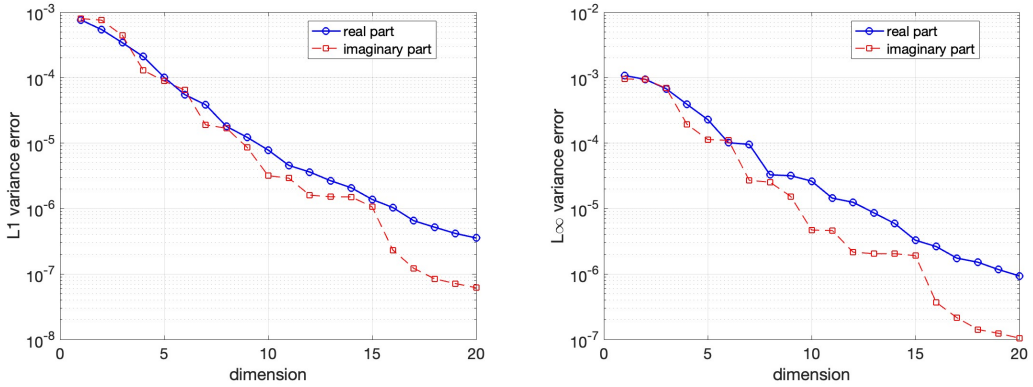

Figure 3.3: Example 2. L_1 (left) and L_∞ (right) errors in the variance of real and imaginary parts of the wave field with respect to the dimension of the random space.

Example 3. In this example, we consider a discontinuous random source f which is given by

$$g(x) = \begin{cases} 0.5, & 0.15 < x < 0.35, \\ 0.5, & 0.65 < x < 0.85, \\ 0, & \text{otherwise}, \end{cases} \qquad h(x) = \begin{cases} 0.5, & 0.3 < x < 0.7, \\ 0, & \text{otherwise}. \end{cases} \tag{3.5}$$

In Figure 3.4, we plot the L_1 and L_∞ errors in the variance of the real and imaginary parts of the wave field with respect to the dimension of the random space. We observe exponential convergence with respect to the dimension of the random space for this example with a discontinuous random source.

3.2 Inverse random source problem

In numerical experiments, the scattering data $u(0, \omega)$ is obtained numerically based on the analytical solution (2.4). To do this, we first evaluate both sides of (2.4) at $x = 0$, yielding

$$u(0, \omega) = \frac{1}{2i\omega} \int_0^1 e^{i\omega y} g(y) dy + \frac{1}{2i\omega} \int_0^1 e^{i\omega y} h(y) dW(y), \tag{3.6}$$

where $dW(y)$ can be truncated as

$$dW(y) \approx \sum_{k=0}^{n} m_k(y) Z_k dy,$$

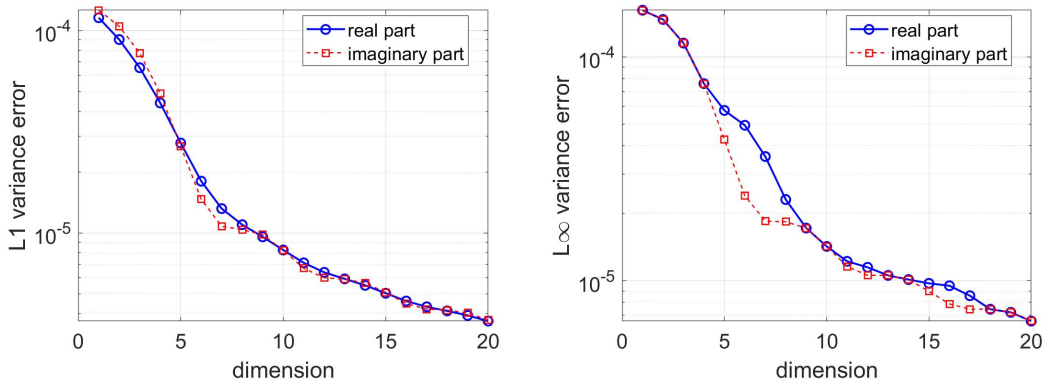

Figure 3.4: Example 3. L_1 (left) and L_∞ (right) errors in the variance of real and imaginary parts of the wave field with respect to the dimension of the random space.

similarly to (2.12), where Z_k are mutually independent standard Gaussian random variables. The real part of $u(0,\omega)$ is given by

$$\Re u(0,\omega) = \frac{1}{2\omega}\int_0^1 \sin(\omega y)g(y)dy + \sum_{k=1}^{n}\left(\int_0^1 \sin(\omega y)h(y)m_k(y)dy\right)Z_k, \tag{3.7}$$

and its gPC coefficients can be approximated numerically by the trapezoidal rule as

$$\Re\hat{u}_0(0,\omega) = \frac{\Delta y}{2\omega}\sum_{i=0}^{K-1}\sin(\omega y_i)g(y_i), \tag{3.8}$$

$$\Re\hat{u}_k(0,\omega) = \frac{\Delta y}{2\omega}\sum_{i=0}^{K-1}\sin(\omega y_i)h(y_i)m_k(y_i), \quad k = 1,2,\ldots,n, \tag{3.9}$$

where $\Delta y = 1/K,\ y_i = i\Delta y = i/K,\ i = 0,1,\ldots,K-1$.

Given the scattering data at a set of frequencies $\omega_j,\ j = 1,\ldots,n_\omega$, we reconstruct the functions $g(x)$ and $h(x)$ in the source function based on the strategy discussed in Section 2.4. We take $m_k(x) = \sqrt{2}\cos((k-1/2)\pi x)$ in the truncation of the white noise defined in (2.12). We set $n = 20$ unless otherwise specified, and take $K = 256$ points for numerical integration. The L_1 error between the reconstructed solution and the exact solution, denoted as "err", is measured over $N_x = 200$ meshes in the spatial domain $(0,1)$.

Remark 1. The scattering data $u(0,\omega)$ is obtained by numerically approximating the solution (3.6) with the gPC expansion in this paper, while the scattering data $u(0,\omega)$ in [6] is obtained by numerically approximating the integrals in (3.6) with the trapezoidal rule

$$u(0,\omega) \approx \frac{1}{2i\omega}\left[\Delta y\sum_{k=0}^{K-1}e^{i\omega y_k}g(y_k) + \sum_{k=0}^{K-1}e^{i\omega y_k}h(y_k)\,dW_k\right], \tag{3.10}$$

where $\Delta y = 1/K, y_k = k\Delta y = k/K$, and $dW_k = \xi_k/\sqrt{K}$ with the set of random samples, $\{\xi_k\}$, being produced from independent standard Gaussian random variables with a mean of zero and a variance of one. The mean and variance of the random source in [6] is recovered with 10^3 and 10^6 samples, while the mean and variance of the random source for the gPC approach discussed in this paper is recovered efficiently with 20 expansions. Thus, the study in [6] is more practical in applications, while our study has a potential for more efficient computation.

Example 1. In this example, the exact mean and variance of the random source function f are given in (3.3). This example is simple since both g and h have a limited number of low-frequency Fourier components.

We use the scattering data $u(0, \omega_k)$ at discrete frequencies $\omega_k = k\pi, k = 1, 2, \ldots, n_\omega$ to reconstruct the mean g and the variance h^2. Figure 3.5 plots the reconstructed mean and variance against the exact ones for different n_ω. We observe that the L_1 error "err" decreases as the number of frequencies n_ω increases, since more scattering data are used in the reconstruction procedure of the stochastic Galerkin method.

We fix the number of frequencies $n_\omega = 40$ and plot the L_1 error between the reconstructed variance and the exact one with respect to the dimension of random variables n in Figure 3.6. We observe that the error decreases gradually as the dimension of the random variable n increases. This indicates that a better reconstruction is obtained when more random variables and thus more terms are used in the truncation of the random process in (2.12). We do not explore the error of the mean function g with respect to n since the mean of the stochastic solution is exactly the first coefficient of the gPC expansion and is independent of n.

Example 2. In this example, the exact mean and variance of the random source function f are given in (3.4). This example is more difficult than Example 1, as both g and h have higher frequency components.

We use the scattering data at discrete frequencies $\omega_k = k\pi$, where $k = 1, \cdots, n_\omega$, to reconstruct the mean g and variance h^2. In Figure 3.7, the reconstructed mean and variance are shown in comparison to the exact ones for different n_ω. We observe that the errors in the mean and variance decrease as the number of frequencies n_ω increases.

Example 3. In this example, the exact mean and variance of the random source function f are given in (3.5). This is a challenging example, as the functions g and h are discontinuous.

We use the scattering data $u(0, \omega_k)$ at discrete frequencies $\omega_k = k\pi, k = 1, \cdots, n_\omega$ to reconstruct the mean g and variance h^2. In Figure 3.8, the reconstructed mean and variance are plotted against the exact ones for different n_ω. It can be observed that the errors of the mean and variance decrease as the number of frequencies n_ω increases, and the oscillatory behavior near the discontinuities is better resolved as n_ω increases. Additionally, we observe the Gibbs phenomenon for this example with discontinuous functions.

4 Conclusion

In this paper, we have demonstrated the application of the stochastic Galerkin method to the direct and inverse random source problems of the one-dimensional Helmholtz equation. The two-point

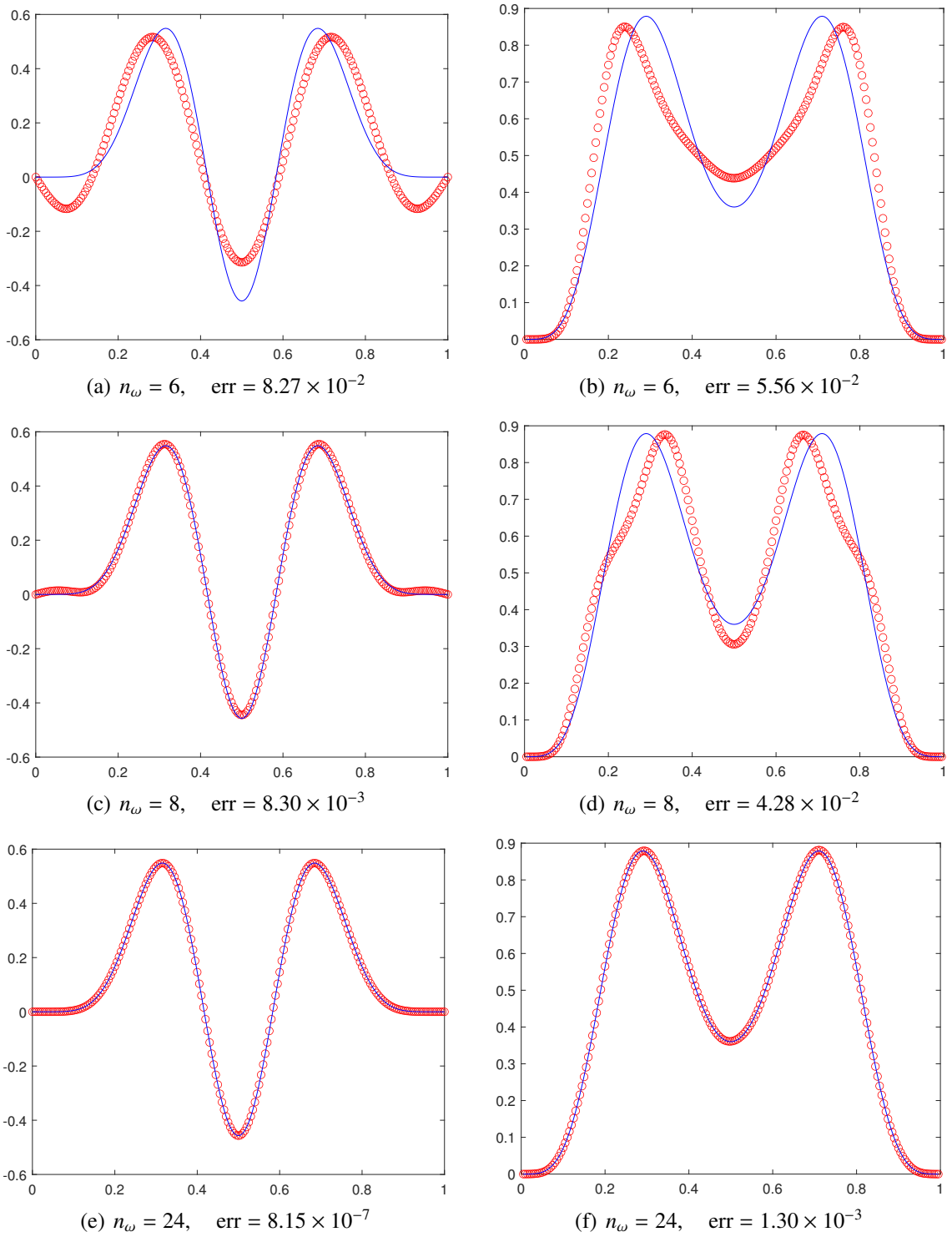

(a) $n_\omega = 6$, err $= 8.27 \times 10^{-2}$ (b) $n_\omega = 6$, err $= 5.56 \times 10^{-2}$

(c) $n_\omega = 8$, err $= 8.30 \times 10^{-3}$ (d) $n_\omega = 8$, err $= 4.28 \times 10^{-2}$

(e) $n_\omega = 24$, err $= 8.15 \times 10^{-7}$ (f) $n_\omega = 24$, err $= 1.30 \times 10^{-3}$

Figure 3.5: Example 1. The mean g (left) and variance h^2 (right) of the exact solutions (solid blue line) and the reconstructed solutions (red circles) with different numbers of frequencies n_ω.

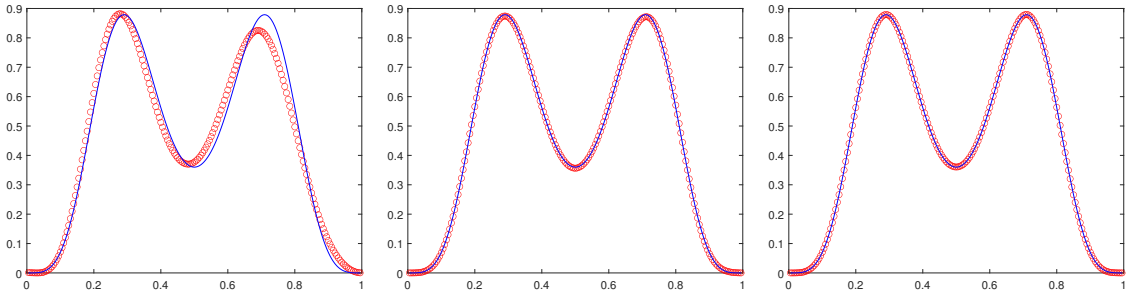

(a) $n = 5$, err $= 3.05 \times 10^{-2}$ (b) $n = 10$, err $= 2.98 \times 10^{-3}$ (c) $n = 20$, err $= 4.20 \times 10^{-4}$

Figure 3.6: Example 1. The variance h^2 of the exact solutions (solid blue line) and the reconstructed solutions (red circles) with respect to the random space dimension n.

stochastic boundary value problem was formulated and solved using the stochastic Galerkin method, yielding an explicit integral representation for the gPC coefficients. It was shown that the gPC coefficients of the zeroth-degree polynomials are related to the sine or cosine transform of the mean of the random source, and the gPC coefficients of the first-degree polynomials are associated with the variance of the random source. The orthogonality of the gPC basis functions enabled the mean and variance of the source to be reconstructed by applying the inverse sine or cosine transform. Furthermore, the gPC coefficients of the second or higher degree polynomials were found to be zero, indicating that the proposed method has the potential to solve a variety of stochastic inverse problems involving high-dimensional random spaces.

Although the random model considered in this work is a Gaussian random process, the method can be applied to inverse random source problems with general stochastic processes. The stochastic Galerkin method is a gPC approximation, where general orthogonal polynomials can be adopted to represent many other random processes. In the context of the gPC approach discussed within this paper, the efficient recovery of the mean and variance of the random source is achievable through a modest number of expansions. Nevertheless, it is important to acknowledge that the current investigation into inverse problems necessitates access to boundary measurements $u(0, \omega, \mathbf{Z})$ at a finite set of angular frequencies. For forthcoming research endeavors, we plan to investigate scenarios wherein boundary measurements are solely available for a limited number of realizations $\mathbf{Z}^{(j)}$, namely, $u(0, \omega, \mathbf{Z}^{(j)})$. The anticipated results are observed from Example 3: exponential convergence for the direct problem and the presence of the Gibbs phenomenon during the treatment of the inverse problem, aligning with the expectations of a spectral approach. As part of our ongoing projects, we intend to explore the incorporation of filters or the concept of domain decomposition for future investigations into inverse problems characterized by various discontinuities. In addition, it presents an interesting topic to study the inverse random source problem within higher dimensions and inhomogeneous background media. We will provide updates on these aspects in the future through other means.

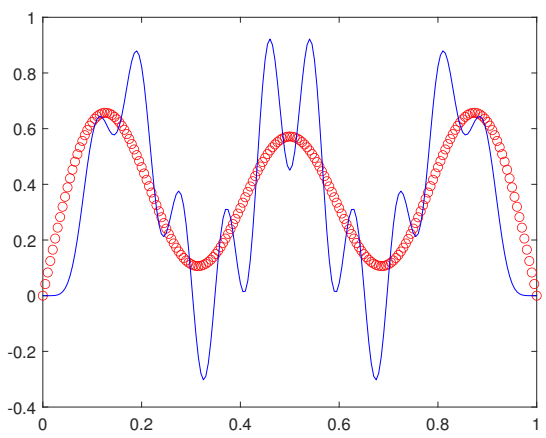

(a) $n_\omega = 6$, err $= 1.77 \times 10^{-1}$

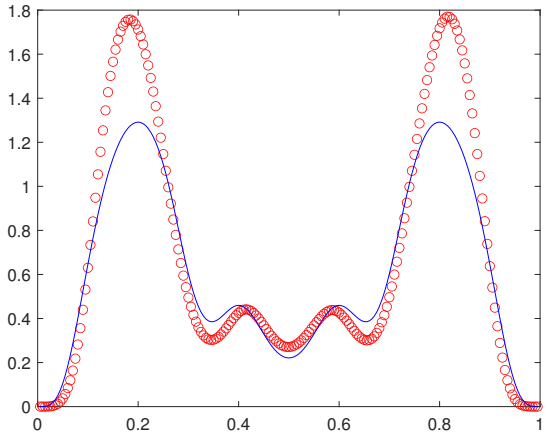

(b) $n_\omega = 6$, err $= 8.02 \times 10^{-2}$

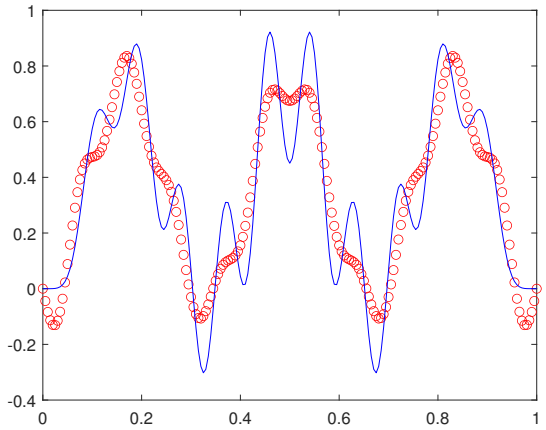

(c) $n_\omega = 22$, err $= 1.19 \times 10^{-1}$

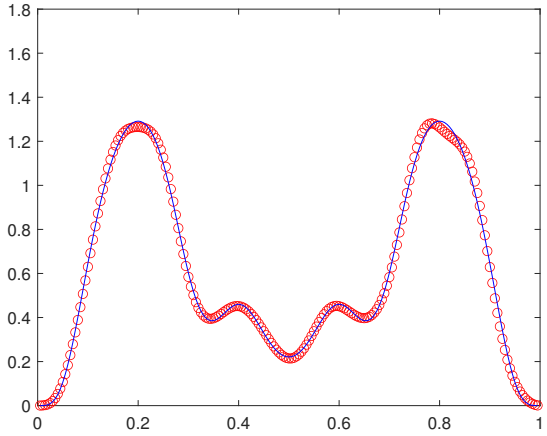

(d) $n_\omega = 22$, err $= 1.02 \times 10^{-2}$

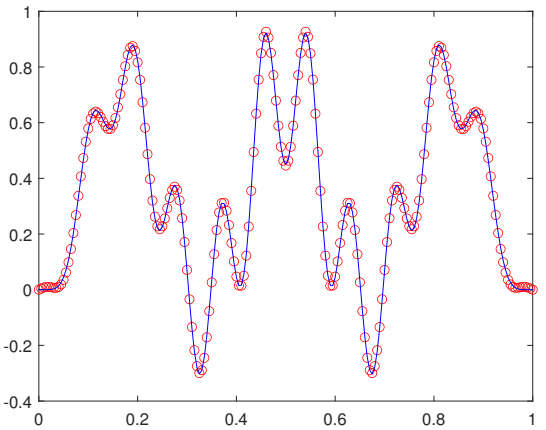

(e) $n_\omega = 26$, err $= 4.10 \times 10^{-3}$

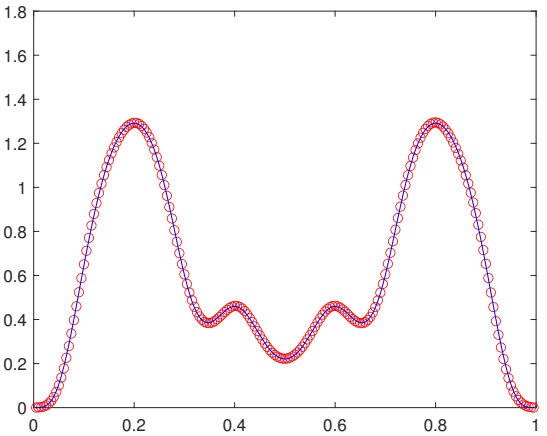

(f) $n_\omega = 26$, err $= 3.20 \times 10^{-3}$

Figure 3.7: Example 2. The mean g (left) and variance h^2 (right) of the exact solutions (solid blue line) and the reconstructed solutions (red circles) with different numbers of frequencies n_ω.

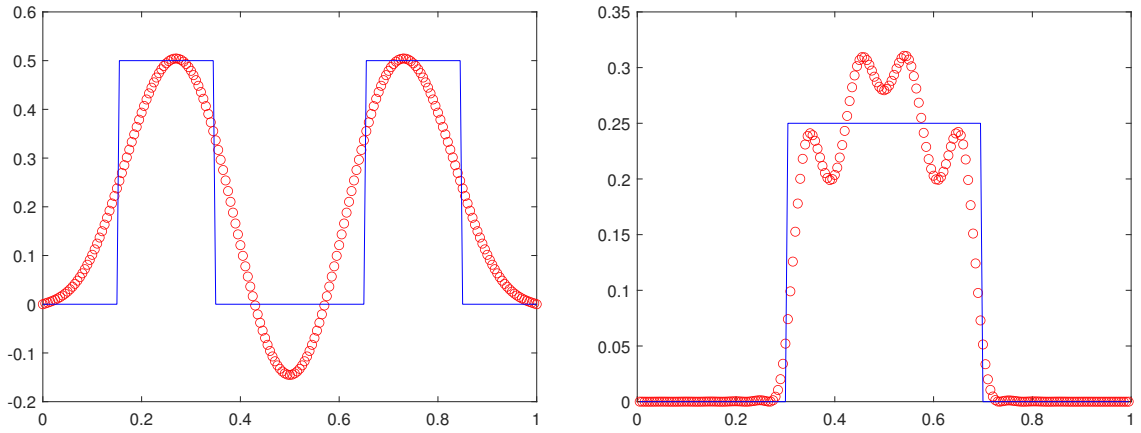

(a) $n_\omega = 6$, err $= 9.57 \times 10^{-2}$

(b) $n_\omega = 6$, err $= 3.23 \times 10^{-2}$

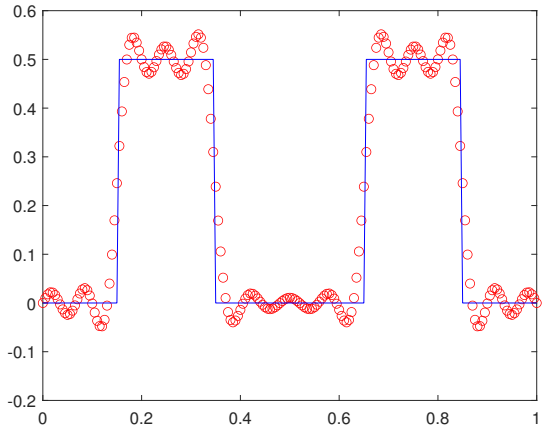

(c) $n_\omega = 28$, err $= 3.45 \times 10^{-2}$

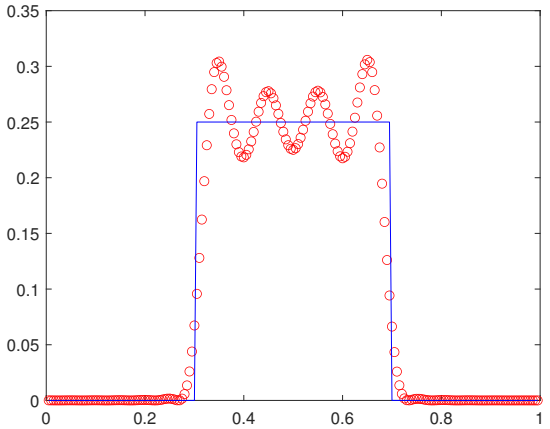

(d) $n_\omega = 28$, err $= 2.73 \times 10^{-2}$

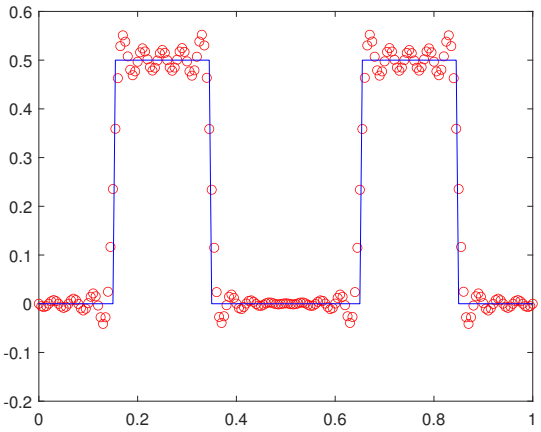

(e) $n_\omega = 50$, err $= 2.25 \times 10^{-2}$

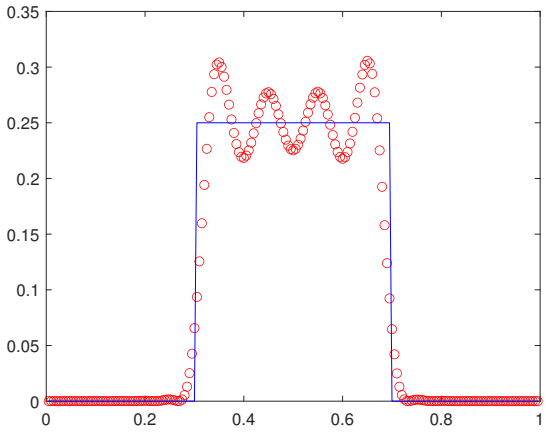

(f) $n_\omega = 50$, err $= 2.70 \times 10^{-2}$

Figure 3.8: Example 3. The mean $g(x)$ (left) and variance $h^2(x)$ (right) of the exact solutions (solid blue line) and the reconstructed solutions (red circles) with different numbers of frequencies n_ω.

Acknowledgments

The research of P. Li was supported in by part the NSF grant DMS-2208256. The research of X. Zhong was partially supported by the NSFC Grant 12272347.

References

[1] R. Albanese and P. Monk, The inverse source problem for Maxwell's equations, Inverse Problems, 22 (2006), 1023–1035.

[2] H. Ammari, G. Bao, and J. Fleming, An inverse source problem for Maxwell's equations in magnetoencephalography, SIAM J. Appl. Math., 62 (2002), 1369–1382.

[3] A. Badia and T. Nara, An inverse source problem for Helmholtz's equation from the Cauchy data with a single wave number, Inverse Problems, 27 (2011), 105001.

[4] M. Badieirostami, A. Adibi, H.-M. Zhou, and S.-N. Chow, Model for efficient simulation of spatially incoherent light using the Wiener chaos expansion method, Optics Letters, 32 (2007), 3188.

[5] G. Bao, C. Chen, and P. Li, Inverse random source scattering problems in several dimensions, SIAM/ASA J. Uncertainty Quantification, 4 (2016), 1263–1287.

[6] G. Bao, S.-N. Chow, P. Li, and H.-M. Zhou, An inverse random source problem for the Helmholtz equation, Math. Comp., 83 (2014), 215–233.

[7] G. Bao, P. Li, J. Lin, and F. Triki, Inverse scattering problems with multi-frequencies, Inverse Problems, 31 (2015), 093001.

[8] G. Bao, J. Lin, and F. Triki, A multi-frequency inverse source problem, J. Differ. Equ., 249 (2010), 3443–3465.

[9] N. Bleistein and J. Cohen, Nonuniqueness in the inverse source problem in acoustics and electromagnetics, J. Math. Phys., 18 (1977), 194–201.

[10] Y. Cao, R. Zhang, and K. Zhang, Finite element method and discontinuous Galerkin method for stochastic Helmholtz equation in two- and three-dimensions, J. Comput. Math., 26 (2008), 701–715.

[11] A. Devaney, The inverse problem for random sources, J. Math. Phys., 20 (1979), 1687–1691.

[12] A. Devaney, E. Marengo, and M. Li, The inverse source problem in nonhomogeneous background media, SIAM J. Appl. Math., 67 (2007), 1353–1378.

[13] M. Eller and N. Valdivia, Acoustic source identification using multiple frequency information, Inverse Problems, 25 (2009), 115005.

[14] J.-P. Fouque, J. Garnier, G. C. Papanicolaou, and K. Sølna, Wave Propagation and Time Reversal in Randomly Layered Media, Stochastic Modelling and Applied Probability, 56, Springer, New York, 2007.

[15] R. G. Ghanem and P. D. Spanos, Stochastic Finite Elements: A Spectral Approach, Springer, New York, 1991.

[16] I. G. Graham, O. R. Pembery, and E. A. Spence, Analysis of a Helmholtz preconditioning problem motivated by uncertainty quantification, Adv. Comput. Math., 47 (2021), 1–39.

[17] J. Kaipio and E. Somersalo, Statistical and Computational Inverse Problems, Springer-Verlag, New York, 2005

[18] G. F. Lawler, Introduction to Stochastic Processes, Chapman and Hall/CRC, New York, 2006.

[19] M. Lassas, L. Päivärinta, and E. Saksman, Inverse scattering problem for a two dimensional random potential, Commun. Math. Phys., 279 (2008), 669–703.

[20] M. Li, P. Li, and C. Chen, Inverse random source scattering for the Helmholtz equation in inhomogeneous media, Inverse Problems, 34 (2018), 015003.

[21] P. Li, An inverse random source scattering problem in inhomogeneous media, Inverse Problems, 27 (2011), 035004.

[22] P. Li and X. Wang, Inverse random source scattering for the Helmholtz equation with attenuation, SIAM J. Appl. Math., 81 (2021), 485–506.

[23] M. Loève, Probability Theory, Springer-Verlag, New York, 1977.

[24] S. Lototsky, R. Mikulevicius, and B. L. Rozovskii, Nonlinear filtering revisited: a spectral approach, SIAM J. Control Optim., 35 (1997), 435–461.

[25] E. A. Spence and J. Wunsch, Wavenumber-explicit parametric holomorphy of Helmholtz solutions in the context of uncertainty quantification, arXiv:2203.10270.

[26] G. Wang, F. Xue, and Q. Liao, Localized stochastic Galerkin methods for Helmholtz problems close to resonance, Int. J. Uncertainty Quantif., 11 (2021), 77–99.

[27] N. Wiener, The Homogeneous Chaos, Am. J. Math., 60 (1938), 897–936.

[28] D. Xiu, Numerical Methods for Stochastic Computations: A Spectral Method Approach, Princeton University Press, 2010.

[29] D. Xiu and G. Karniadakis, The Wiener–Askey polynomial chaos for stochastic differential equations, SIAM J. Sci. Comput., 24 (2002), 619–644.

[30] Z. Zhang and G. E. Karniadakis, Numerical Methods for Stochastic Partial Differential Equations with White Noise, Applied Mathematical Sciences, vol. 196, Springer, Heidelberg/Berlin, Germany, 2017.